of order unity given by the ratio $M_\infty^2/\overline{Re}_{x_\infty}$, thus providing an alternative interpretation for this rarefaction parameter.

4. Comparison with Experiment

Perhaps the most interesting property of the Knudsen number $\lambda_s/\delta^* = F(\gamma)M_\infty^2/\overline{Re}_{x_\infty}$ is that it is to first order independent of the temperature of the wall. It follows, therefore, that, if this Knudsen number is an appropriate one for correlating the first appearances of slip effects in the vicinity of the leading edge, the correlation should apply both to the cold-wall flows obtained in shock tunnels and the adiabatic-wall flows obtained in unheated low-density wind tunnels, and that the correlation should apply to both surface pressures and heat transfer. As will be seen, the existing experimental data support this conjecture.

The first observations of slip effects near the leading edge were obtained by Schaaf et al.[1] in their measurements of surface pressure distributions. These measurements were obtained in the unheated Berkeley low-density wind tunnel, at Mach numbers ranging from 3.7 to 5.8, with adiabatic wall conditions. Within the scatter of these data, one may estimate that the first significant departures from strong interaction theory occur at values of around $M_\infty/(\overline{Re}_{x_\infty})^{1/2}$ between 0.2 and 0.3. More recently, Vidal and Wittliff[4] have reported surface pressure and heat transfer measurements obtained in the Cornell Aeronautical Laboratory low-density shock tunnel. These tests were in the Mach number range $14 < M_\infty < 22$ and under cold-wall conditions where the wall temperature/stagnation temperature ratio was in the range $0.07 < T_b/T_0 < 0.10$. These authors, in fact, show that the departures of their data from interaction theory could be correlated with the parameter $M_\infty/(\overline{Re}_{x_\infty})^{1/2}$. They found that the departures from strong interaction theory occurred at about $M_\infty/(\overline{Re}_{x_\infty})^{1/2} \sim 0.3$ for the heat transfer, and at about $M_\infty/(\overline{Re}_{x_\infty})^{1/2} \sim 0.1$ for the surface pressure. It is significant that these values agree, probably within the accuracy of the several experiments, with the Berkeley data. The agreement is surprisingly good, when one considers the quite different flow conditions involved. Slip effects also have been observed by Nagumatsu et al.,[2, 3] but unfortunately these data have a little too much scatter to permit accurate estimates of the value of $M_\infty/(\overline{Re}_{x_\infty})^{1/2}$ at which slip effects appear.

To summarize, it appears that the parameter $M_\infty/(\overline{Re}_{x_\infty})^{1/2}$ is appropriate for correlating the emergence of slip-flow effects near the leading edge of a flat plate in hypersonic flow. According to the first interpretation that has been given to this parameter, in terms of the Knudsen number λ_s/δ^*, slip effects become important at about $\lambda_s/\delta^* \sim 0.01$, which is also the value of $(\lambda/\delta^*)_{\text{low speed}}$ usually cited for the beginning of the low-speed slip-flow regime. According to the alternative interpretation of the parameter $M_\infty/(\overline{Re}_{x_\infty})^{1/2}$ in terms of the δ_m/x, slip effects appear when distance from the leading edge is less than roughly 10 times the shock thickness. Another demonstration is seen here of the fact that, when slip effects become important in the leading edge region, the shock wave no longer can be treated as a discontinuity.

References

[1] Schaaf, S. A., Hurlbut, F. C., Talbot, L., and Aroesty, J., "Viscous interaction experiments at low Reynolds numbers," ARS J. **29**, 527–528 (1959).

[2] Nagamatsu, H. T., Sheer, R. E., and Schmid, J. R., "High temperature rarefied hypersonic flow over a flat plate," ARS J. **31**, 902–910 (1961).

[3] Nagamatsu, H. T., Weil, J. A., and Sheer, R. E., Jr., "Heat transfer to flat plate in high temperature rarefied ultrahigh Mach number flow," ARS J. **32**, 533–541 (1962).

[4] Vidal, R. J. and Wittliff, C. E., "Hypersonic low-density studies of blunt and slender bodies," *Proceedings of the Third International Symposium on Rarefied Gas Dynamics*, edited by J. A. Laurmann (Academic Press Inc., New York, to be published).

[5] Hayes, W. D. and Probstein, R. F., *Hypersonic Flow Theory* (Academic Press Inc., New York, 1959), Chap. 9.

[6] Talbot, L., "Survey of the shock structure problem," ARS J. **32**, 1009–1016 (1962).

Effects of Winds Aloft on Loads of the Dyna-Soar Booster

R. P. McFarland* and J. H. Robertson Jr.†
The Martin Company, Baltimore, Md.

THIS note presents the effects of winds aloft on the loads of a preliminary configuration Dyna-Soar booster, which was a modified Titan II missile with a glider at the forward end and large stabilizing fins at the aft end. The addition of the winged glider and fins provided large aerodynamic lifting surfaces that induced loads in the booster, under the influence of winds aloft.

Figure 1 shows the modified AviDyne 1% risk winds[1] used in the preliminary design of the booster. The maximum 1% envelope is used in conjunction with the 3000-ft wind shear data to construct discrete windspeed profiles similar to the ones illustrated for 25,000-, 30,000-, and 35,000-ft altitudes. The discrete wind profile to be applied, then, consists of the minimum windspeed curve, up to an altitude 3000 ft below the altitudes of interest, a 3000-ft wind shear to the maximum 1% envelope, a shear reversal of 3000 ft back to the minimum curve, and the minimum curve for the balance of the altitude range.

The discrete profiles shown in Fig. 1 are valid only for tailwinds. For application of other winds, such as sidewinds and headwinds, Fig. 2 illustrates the normalized wind rose,[2] which relates wind magnitude with direction. The wind rose is considered constant with altitude and is based on a tailwind for an easterly launch azimuth. Therefore, discrete windspeed profiles can be constructed for any wind direction by applying the wind rose of Fig. 2 to the maximum 1% envelope of Fig. 1. The wind shear data of Fig. 1 are considered applicable for any wind direction.

The relative bending moments of Fig. 3 show the bending moments associated with analytical flights through the discrete windspeed profiles of Fig. 1. Two different load analyses considered the response of the vehicle to a 3000-ft wind shear reversal at an altitude of 35,000 ft. (This altitude was found to be representatively critical for inducing lateral loads of a vibratory nature.) The dynamic analysis considered five degrees of freedom: rigid body rotation, rigid body translation, and the first three structural modes. In addition, consideration in this analysis was given to the dynamic characteristics of the autopilot and control systems. The pseudostatic load analysis essentially set all modal velocity and acceleration terms to zero. In doing this, velocities and accelerations were considered only in the rigid body modes of the vehicle.

A comparison of the data of Fig. 3 illustrates the adequacy of the pseudostatic analysis. Although the maximum dynamic bending moment did not occur at the point of windspeed shear reversal, as was the case of the pseudostatic

Presented at the ARS Launch Vehicles: Structures and Materials Conference, Phoenix, Ariz., April 3–5, 1962; revision received January 4, 1963.

* Group Engineer, Structures and Materials Department. Member AIAA.

† Associate Engineer, Structures and Materials Department. Associate Member AIAA.

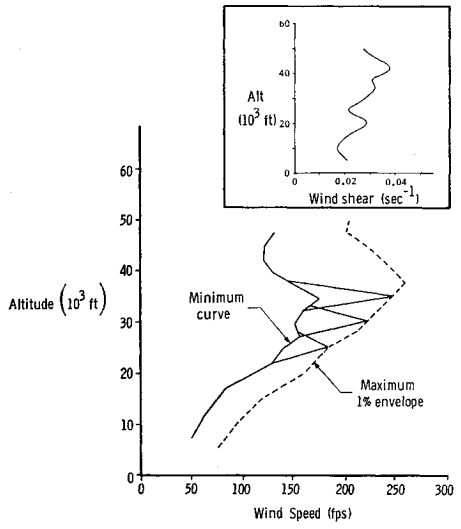

Fig. 1 Modified AviDyne 1% risk wind and wind shear

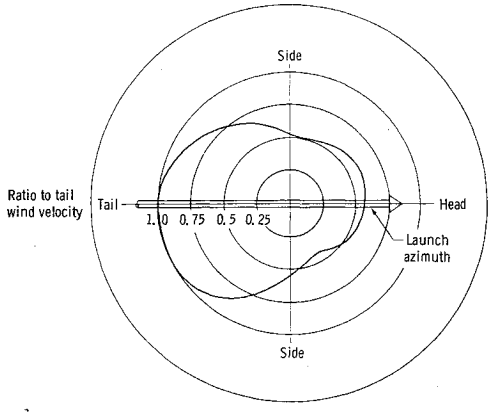

Fig. 2 Normalized wind rose

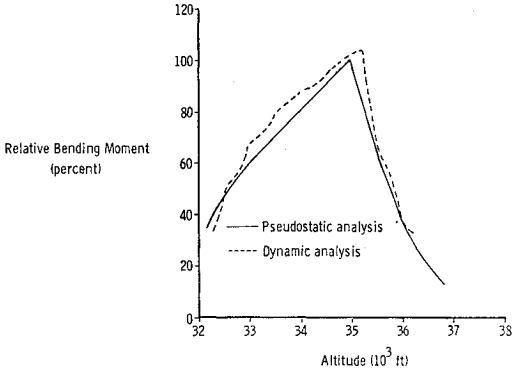

Fig. 3 Dynamic-pseudostatic moment analyses

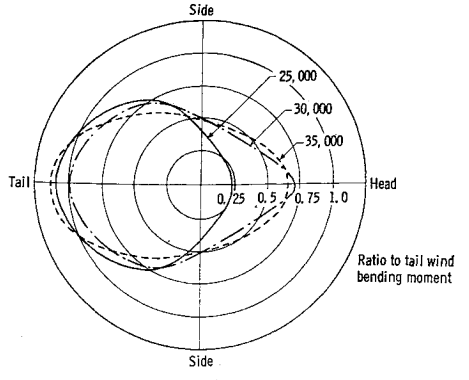

Fig. 4 Composite moment rose for wind shear reversals at 25,000, 30,000, and 35,000 ft

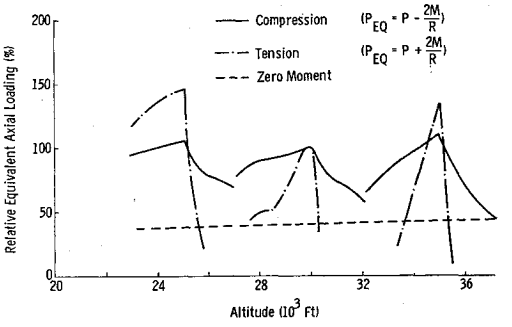

Fig. 5 Relative equivalent axial loading

analysis—and was 4% in excess of the pseudostatic loading—accuracies of these magnitudes are considered adequate.

Therefore, the loads arising from the application of the wind data of Figs. 1 and 2 to the preliminary configuration Dyna-Soar booster may be assessed, considering only the quasi-steady-state motion of the vehicle and the ensuing pseudostatic loading. The vehicle was flown analytically through the discrete windspeed profiles illustrated in Fig. 1 with wind directions that varied from tailwinds through sidewinds to headwinds. The bending moment histories of representatively critical areas on the booster were determined. The variation of the maximum bending moments with wind aximuth for one such area is shown in Fig. 4, which shows that maximum lateral loads occur for a tailwind at an altitude of 35,000 ft.

However, bending moments alone do not necessarily determine the design criticality of the structure and must be considered in conjunction with other loadings. A measure of the design criticality is the equivalent axial load, which is defined as that axial load that results in a uniform stress distribution around the periphery of a monocoque cylinder, equal to the maximum stress under the combined action of bending moment and axial load, or

$$P_{EQ} = P \pm (2M/R)$$

where P_{EQ} = equivalent axial load, M = moment, P = axial load, and R = vehicle radius.

Figure 5 shows the compression and tension equivalent axial loads associated with tailwind loading. These curves are relative to their respective 30,000-ft peak values. It may be seen readily that the maximum compression equivalent axial load occurs at 35,000 ft. However, when the tension equivalent axial load is considered, the maximum loading occurs at the 25,000-ft altitude. This indicates that the interaction of axial loads and bending moments can produce maximum tension loading at a point along the trajectory when the bending moment is less severe than its maximum value.

The effects of the AviDyne 3000-ft wind shears and discrete windspeed profiles on the loads associated with the preliminary configuration booster have been determined. The application of wind shears over depths other than 3000 ft must be considered to assure that the 3000-ft shear produces maximum loads and that no adverse structural resonances are induced.

A study was conducted to determine the effects of the wind shear reversal and its characteristics on the vehicle's loads. The study determined the effects of wind shear, velocity, and shear depth on the bending moments at the 35,000-ft altitude. The study used dynamic analyses and reflects the elastic structure coupled with the autopilot and control system. The results are shown in Figs. 6 and 7. In each instance, the vehicle was flown through the wind shear reversal under the same initial conditions.

Figure 6 illustrates the variation of the maximum relative bending moment with shear depth, for constant wind velocity increment. The maximum bending moment associated with a 90-fps velocity increment over a shear depth of 3000

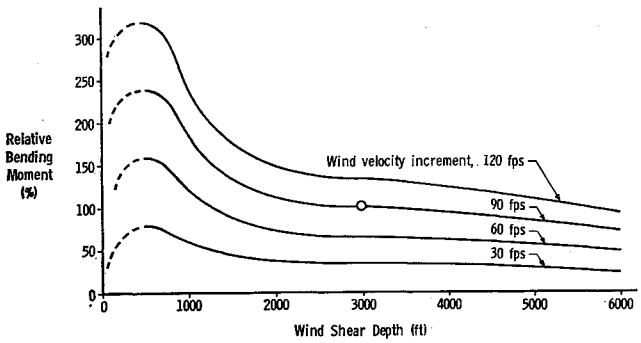

Fig. 6 Variation of relative bending moment with shear depth for constant wind velocity

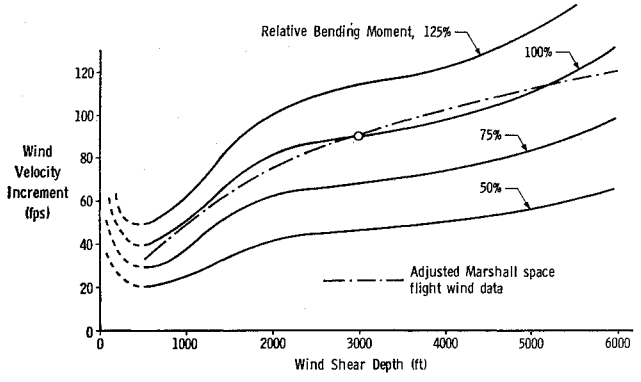

Fig. 7 Variation of wind velocity with shear depth for constant relative bending moment

ft was selected as the 100% level. The effects of the characteristics of an arbitrary wind shear reversal can be assessed from these data. Changes in wind velocity increment or shear depth can be expressed in terms of an increase or decrease in bending moment. The combinations of wind velocity increment and shear depth that produce the same relative bending moment level are presented in Fig. 7.

The wind velocity increments associated with shear depths other than 3000 ft have been determined for the 10- to 14-km region.[3] Normalizing the magnitudes of these velocity increments about the 3000-ft value will give the variation of wind velocity for depths other than 3000 ft. The dotted portion of the data in Fig. 7 is based on these adjusted variations of velocity increment with shear depth, the basis being an increment of 90 fps over a depth of 3000 ft.

Comparison of the adjusted data of Fig. 7 with 100% load level indicates that the 3000-ft shear depth does not produce critical loading. The critical depth lies between 3000 and 5200 ft, at approximately 4000 ft, which corresponds to a relative bending moment of about 105%.

The study illustrates that the maximum loading occurred at a depth in excess of 3000 ft, which demonstrates that wind criteria established to produce a given risk in terms of structural capability are vulnerable to changes in configuration, flight control system, etc. However, it does show that such criteria are adequate in the design of R&D boosters, since launch dates can be selected.

References

[1] Hobbs, N. P., Criscione, E. S., Mazzola, L. L., and Frassinelli, G. J., "Development of interim wind shear and gust design criteria for vertically rising vehicles" (unclassified title), Wright Air Dev. Center TR 59-504, AviDyne Research Inc. (July 1959).

[2] Easley, J. W. and Walkenhorst, W. F., "Approach to development of comprehensive wind design criteria," *Proceedings of the National Symposium on Winds for Aerospace Vehicle Design* (Geophys. Res. Dir., Air Force Cambridge Res. Labs., L. G. Hanscom Field, Bedford, Mass., 1962), Vol. 2, no. 140, pp. 103–118.

[3] Scoggins, J. R. and Vaughan, W. W., "Cape Canaveral wind and shear data (1 through 80 km) for use in vehicle design and performance studies," NASA TN D1274 (July 1962).

Rarefied-Gas Field Equations for Plane Shear Disturbance Propagation

J. G. Logan*
Aerospace Corporation, Los Angeles, Calif.

In a recent note,[1] the two-dimensional linearized Grad equations for the rarefied-gas field, when applied to the Rayleigh problem, were shown to yield the following characteristic equations for the propagation of small shear disturbances:

$$\left[\frac{\partial}{\partial t} \pm \left(\frac{7}{5}\right)^{1/2} \frac{\partial}{\partial y}\right] Q_{\pm}(y, t) = -\frac{L}{t_f c_0}\left[\frac{P_{xy}}{p_0} \pm \frac{4}{3(35)^{1/2}} \frac{q_x}{p_0 c_0}\right] \quad (1)$$

where the propagating quantity Q is given by

$$Q_{\pm} = \left[\frac{P_{xy}}{p_0} \pm \left(\frac{u}{c_1} + \frac{2}{5}\frac{q_x}{p_0 c_1}\right)\right]$$

P_{xy} is the shear stress, u the disturbance velocity, q_x the heat flux, c_1 the propagation velocity defined by

$$c_1 = (\tfrac{7}{5})^{1/2} c_0 = (\tfrac{7}{5} R T_0)^{1/2} \qquad c = c_1/c_0$$

p_0 is the equilibrium pressure and T_0 the equilibrium temperature. The relaxation time is defined by $t_f \simeq \mu_0/p_0$, i.e., the ratio of viscosity to pressure.

In the limit $t_f \gg L/c_0$, Eq. (1) can be written as

$$[(\partial/\partial t) \pm c(\partial/\partial y)]Q_{\pm} = 0 \quad (2)$$

Consequently, in the limit of large relaxation time, plane shear disturbances initiated by field particle collisions with a boundary will propagate unchanged through the field.

As an illustrative example, the disturbance produced by the impulsive motion of an infinite plate in a rarefied-gas field, initially in equilibrium at a temperature T_0, can be calculated assuming that specular reflection does not occur at the boundary (Fig. 1). The field particles are absorbed and reemitted with a Maxwellian distribution at the temperature T_0 and the shear velocity U. Hence,

$$Q_{+} = \frac{P_{xy}}{p_0} + \frac{u}{c_1} + \frac{2}{5}\frac{q_x}{p_0 c_1} = \frac{U}{c_1} \qquad P_{xy} = q_x = 0$$

The complimentary characteristic quantities for the small longitudinal disturbances[1] yield $P_{1+} = P_{2+} = 0$, where

$$P_{1+} = \theta - 0.51p - 0.11\frac{P_{yy}}{p_0} + 0.33\frac{q_y}{p_0 c_0} - 0.42\frac{v}{c_0}$$

$$P_{2+} = \theta + 0.78p + 1.18\frac{P_{yy}}{p_0} + 0.85\frac{q_y}{p_0 c_0} + 1.66\frac{v}{c_0}$$

When the disturbance Q reaches boundary (B), Fig. 1, the following mass, momentum, and energy conditions must be satisfied:[2]

$$p + \tfrac{1}{2}(P_{yy}/p_0) = s_w \quad (3)$$

$$\frac{P_{xy}}{p_0} + 0.16\frac{q_x}{p_0 c_0} = 0.8\frac{U}{c_0} + 0.4\frac{P_{yy}}{p_0}\frac{U}{c_0} \approx 0.8\frac{U}{c_0} \quad (4)$$

$$(P_{yy}/p_0) + 2.51(q_y/p_0 c_0) = (U/c_0)^2 \quad (5)$$

on assuming a wall condition such that $\theta = \theta_w = 0$ and $u = 0$.

Received by IAS November 26, 1962; revision received January 2, 1963.

* Director, Aerodynamics and Propulsion Research Laboratory. Member AIAA.